Article

# Preparation and Properties of Metallic, Superhard Rhenium Diboride Crystals

Jonathan B. Levine, Sandy L. Nguyen, Haider I. Rasool, Jeffrey A. Wright, Stuart E. Brown, and Richard B. Kaner

*J. Am. Chem. Soc.*, **2008**, 130 (50), 16953-16958 • DOI: 10.1021/ja804989q • Publication Date (Web): 18 November 2008



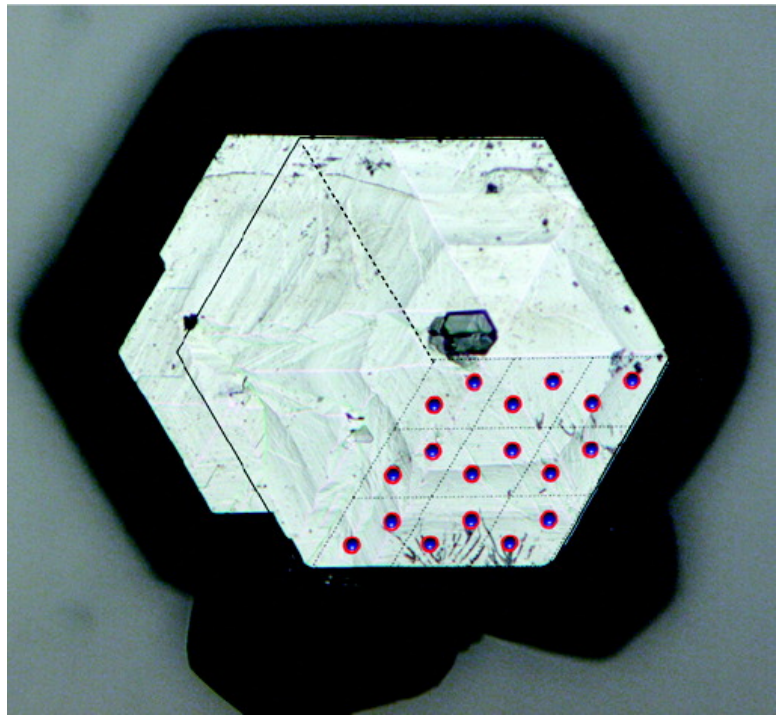

J|A|C|S
ARTICLES

Published on Web 11/18/2008

# Preparation and Properties of Metallic, Superhard Rhenium Diboride Crystals

Jonathan B. Levine,[†] Sandy L. Nguyen,[†] Haider I. Rasool,[†] Jeffrey A. Wright,[‡] Stuart E. Brown,[‡,§] and Richard B. Kaner*[,†,§]

*Department of Chemistry & Biochemistry and Department of Physics & Astronomy, University of California, Los Angeles, Los Angeles, California 90095*

Received June 30, 2008; E-mail: kaner@chem.ucla.edu

***Abstract:*** Single crystals of $ReB_2$ have been prepared from an aluminum flux under inert gas flow. The crystals are typically 1−3 mm in diameter and 500 $\mu$m thick, growing along the [002] direction with a distinct hexagonal morphology. Vickers microhardness and nanoindentation testing indicate that the (002) plane possesses the highest hardness with measured values of 40.5 and 36.4 GPa, respectively. The elastic anisotropy was examined and the indentation moduli of the basal plane and an (*hk*0) plane of unknown indices are 675 and 510 GPa, respectively. Four-probe electrical resistivity measurements demonstrate that $ReB_2$ is the hardest material known to exhibit metallic behavior. Thermogravimetric analysis indicates that the crystals are stable in air up to 1000 °C due to the formation of a protective boron oxide coating.

## Introduction

The binary transition metal borides have been the focus of attention for decades because of their useful mechanical and electrical properties.[1] $MgB_2$, for example, has been reported to be superconducting at 39 K.[2] Additionally, $HfB_2$, $ZrB_2$, and $TiB_2$ exhibit high hardness and good thermal stability,[3−5] and $OsB_2$ is ultra-incompressible.[6] Rhenium diboride, originally synthesized in the 1960s,[7] is a refractory compound with a melting point of 2400 °C[8] that was reported by our group to be an ultra-incompressible, superhard material (hardness ≥ 40 GPa).[9] Recently, thin films of $ReB_2$ were prepared by pulsed laser deposition that were also shown to be superhard.[10] Since our initial publication, there have been several theoretical studies reported on the electrical, thermal, and rheological properties of $ReB_2$ to better understand this material's unique combination of properties.[11−17] To date, $ReB_2$ crystals have been synthesized by arc melting, by zone melting, and using an optical floating zone furnace.[9,18,19] However, an extended study of the physical properties of $ReB_2$ has not been performed.

The use of single crystals is important for measuring the intrinsic properties of a material, as these properties are altered by grain boundaries in polycrystalline samples. Furthermore, because the layered crystal structure of $ReB_2$ lends itself to anisotropy, its physical properties, such as hardness, vary with crystallographic orientation. Measurements performed on single crystals allow separate characterization of a material's individual lattice planes. Knowledge of the mechanical anisotropy of a material is also potentially useful for applications and effective theoretical modeling of superhard materials. Here, we report the synthesis and characterization of $ReB_2$ single crystals grown by a flux technique.

## Experimental Section

**Synthesis.** Powders of rhenium metal (Rhenium Alloys, Inc., 99.99%) and amorphous boron (Cerac, Inc., 99.9%) were added to an alumina crucible containing an excess of aluminum (Cerac, 99.999%) as the growth medium. Using 2 g of Re, the molar ratio of Re/B/Al was fixed at 1:2:50. The crucible was covered and placed in an alumina tube in a resistively heated furnace with flowing Ar gas. The furnace was heated to 1400 °C at a rate of 100 °C/h, held there for 5 h, slowly cooled to 700 °C at a rate of 10 °C/h, and

[†] Department of Chemistry & Biochemistry.
[‡] Department of Physics & Astronomy.
[§] California NanoSystems Institute.

(1) Aronsson, B.; Lundström, T.; Rundqvist, S. *Borides, Silicides, and Phosphides*; Methuen: London, 1965.
(2) Nagamatsu, J.; Nakagawa, N.; Muranaka, T.; Zenitani, Y.; Akimitsu, J. *Nature* **2001**, *410*, 63–64.
(3) Kalish, D.; Clougherty, E. V.; Kreder, K. *J. Am. Ceram. Soc.* **1969**, *52*, 30–36.
(4) Bsenko, L.; Lundström, T. *J. Less-Common Met.* **1974**, *34*, 273–278.
(5) Munro, R. G. *J. Res. Natl. Inst. Stand. Technol.* **2000**, *105*, 709–720.
(6) Cumberland, R. W.; Weinberger, M. B.; Gilman, J. J.; Clark, S. M.; Tolbert, S. H.; Kaner, R. B. *J. Am. Chem. Soc.* **2005**, *127*, 7264–7265.
(7) La Placa, S.; Post, B. *Acta Crystallogr.* **1962**, *15*, 97.
(8) Okamoto, H. *Phase Diagrams for Binary Alloys, Desk Handbook*; 2000; Vol. 1.
(9) Chung, H.-Y.; Weinberger, M. B.; Levine, J. B.; Kavner, A.; Yang, J.-M.; Tolbert, S. H.; Kaner, R. B. *Science* **2007**, *316*, 436–439.
(10) Latini, A.; Rau, J. V.; Ferro, D.; Teghil, R.; Albertini, V. R.; Barinov, S. M. *Chem. Mater.* **2008**, *20*, 4507–4511.
(11) Zhang, R. F.; Veprek, S.; Argon, A. S. *Appl. Phys. Lett.* **2007**, *91*, 201914/1–201914/3.
(12) Zhou, W.; Wu, H.; Yildirim, T. *Phys. Rev. B: Condens. Matter* **2007**, *76*, 184113/1–184113/6.
(13) Liang, Y.; Zhang, B. *Phys. Rev. B: Condens. Matter* **2007**, *76*, 132101/1–132101/4.
(14) Chen, X.-Q.; Fu, C. L.; Krcmar, M.; Painter, G. S. *Phys. Rev. Lett.* **2008**, *100*, 196403/1–196403/4.
(15) Hao, X. F.; Xu, Y. H.; Wu, Z. J.; Zhou, D. F.; Liu, X. J.; Cao, X. Q.; Meng, J. *Phys. Rev. B* **2006**, *74*, 224112.
(16) Hao, X. F.; Wu, Z. J.; Xu, Y. H.; Zhou, D. F.; Liu, X. J.; Meng, J. *J. Phys.: Condens. Matter* **2007**, *19*, 196212.
(17) Wang, Y. X. *Appl. Phys. Lett.* **2007**, *91*, 101904.
(18) Lyashchenko, A. B.; Paderno, V. N.; Filippov, V. B.; Borshchevskii, D. F. *Sverkhtverd. Mater.* **2006**, 79–81.
(19) Otani, S.; Aizawa, T.; Ishizawa, Y. *J. Alloys Compd.* **1997**, *252*, L19–L21.

  

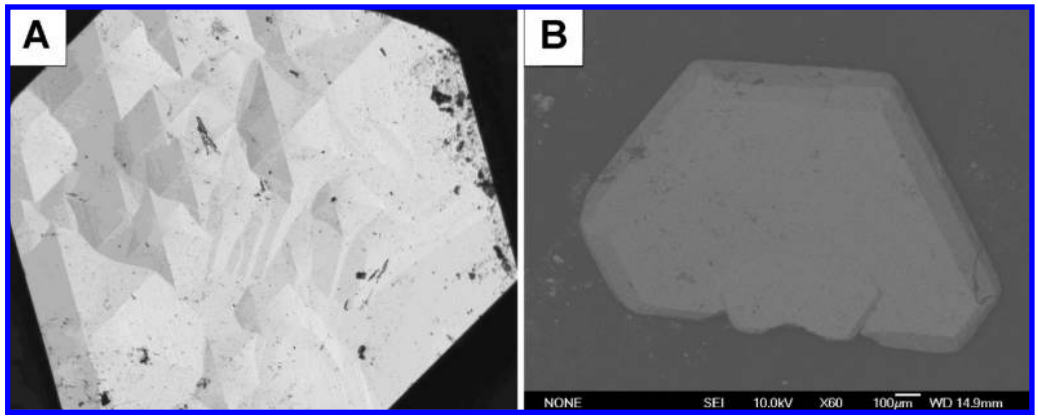


***Figure 1.*** (A) Optical image of an as-grown $ReB_2$ crystal synthesized in an aluminum flux. Hexagonal growth patterns are clearly visible on the crystal surface. (B) Scanning electron micrograph image of a $ReB_2$ crystal grown in an aluminum flux (scale bar = 100 $\mu$m).

then quickly cooled to room temperature. The aluminum flux was then dissolved in 6 M NaOH, and the resulting products were filtered with deionized water and dried in air.

**Characterization.** Powder X-ray diffraction patterns were collected on a XPert Pro powder diffractometer with Cu K$\alpha$ radiation ($\lambda$ = 1.5418 Å; PANalytical). The crystal faces were indexed on a SMART 1000/APEX II single crystal diffractometer (Bruker Corp.). Electron micrograph images were collected using a JSM-6700F field emission scanning electron microscope (JEOL Ltd.). Thermal stability measurements were collected on a Pyris Diamond TG/DTA (Perkin-Elmer Instruments) between 23 and 1000 °C with a heating rate of 10 °C/min. For indentation measurements, the samples were encased in a slow-curing epoxy resin and preliminary polishing was carried out using silicon carbide abrasive paper. Diamond films (30, 15, 6, 3, and 1 $\mu$m particle sizes) were used for fine polishing in order to obtain a mirror finish. Microindentation experiments were performed on a Vickers diamond microindenter (Buehler Ltd.). Fifteen indents were made with a Vickers indenter at each load, beginning with 4.9 N and ending at 0.49 N, to ascertain the load-dependent hardness. The indentation diagonal lengths were measured using an Axiotech 100 reflected-light microscope (Carl Zeiss, Inc.) under 500× magnification. Digital images were taken using an attached AxioCam MRc color CCD camera (Carl Zeiss). Nanoindentation was performed using a Nano Indenter XP with a Berkovich diamond indenter (MTS Systems Corp.). Hardness values were calculated *in situ* according to the method developed by Oliver and Pharr.[20]

Electrical resistivity measurements were performed on a polished crystal 800 $\mu$m × 1600 $\mu$m × 700 $\mu$m using a standard four-probe configuration. The probes were attached to the (002) face and data were collected upon heating from 12.5 to 300 K. Magnetic susceptibility measurements were made using a Magnetic Properties Measurement System (Quantum Design, Inc.) in a direct current field from 2 to 300 K.

## Results and Discussion

**Structure Analysis.** Crystals obtained from the aluminum flux have well-defined hexagonal symmetry, and the largest crystals grow to a maximum size of 3 mm in diameter and 1 mm thickness (Figure 1). The hexagonal faces, clearly visible in Figure 1A, indicate that the crystals grow primarily along the *c*-axis. The crystal growth does not go to completion, as indicated by the presence of $ReB_2$ powder along with the formed crystals.

Powder diffraction measurements were taken on pulverized $ReB_2$ crystals and indexed, using silicon (Cerac, 99.999%) as an internal standard. The powder pattern was matched to JCPDS file 00-011-0581, confirming the growth of $ReB_2$ crystals (Figure 2A). The lattice parameters were determined by Rietveld refinement with the JADE software package (version 6.0), and the values are in good agreement with those originally reported by La Placa and Post,[7] $a$ = 2.897(2) Å, $c$ = 7.472(4) Å, with a final $R_{wp}$ of 12.75%. The slightly high value for the *R*-factor can be attributed to preferred orientation effects of the crushed crystals. This report presents the first synthesis of any superhard material by flux crystal growth under ambient pressure.

Powder X-ray diffraction was also collected on the as-grown crystals oriented such that the hexagonal faces were parallel to the horizontal plane of the diffractometer in order to confirm that the crystals grow along the *c*-axis. Figure 2B shows the X-ray pattern for the as-grown crystal. Only three peaks are present, corresponding to the (002), (004), and (006) planes, demonstrating that the (00*l*) plane grows outward. This growth pattern leads to the formation of hexagonal platelets oriented perpendicularly to the *c*-axis. Attempts to refine the unit cell using single crystal diffraction were unsuccessful because of the large degree of twinning present in the crystals (observed in Figure 1A), which are most likely due to 60° rotations in the *ab* plane during the growth process. However, the terminating crystallographic planes present on the surface of the crystals as shown in Figure 3 provide further evidence that the crystals grow along the *c*-axis. Previously, $ReB_2$ synthesized in an optical floating zone (FZ) furnace was reported to grow in the (00*l*) direction, in agreement with our own observations.[19]

**Chemical Analysis.** Chemical analysis was performed using inductively coupled plasma atomic emission spectroscopy (ICP-AES). The nominal composition of $ReB_2$ was determined to have a true composition of $ReB_{1.85}$. This value is in good agreement with the reported analytically determined value of $WB_{1.85}$ for "$WB_2$" crystals grown in an aluminum flux.[21] The boron-deficient composition of the diboride crystals provides confirmation for the defective nature of the puckered boron layers that exist in both compounds.[7,22,23] The composition of arc-melted $ReB_2$ was analyzed as a control and determined to form in a 1:2 ratio. $ReB_2$ crystals grown in the FZ furnace were also shown to be of stoichiometric composition, as determined by ICP-AES.[19] The boron-deficient nature of our $ReB_2$ crystals is then a direct result of growing the crystals in a metal flux and may be responsible for the lower hardness values discussed below.

(20) Oliver, W. C.; Pharr, G. M. *J. Mater. Res.* **1992**, *7*, 1564.
(21) Okada, S.; Kudou, K.; Lundstrom, T. *Jpn. J. Appl. Phys., Part 1* **1995**, *34*, 226–31.
(22) Lundström, T. *Acta Chem. Scand.* **1968**, *22*, 2191–2199.
(23) McColm, I. J. *Ceramic Hardness*; Plenum Press: New York, 1990.

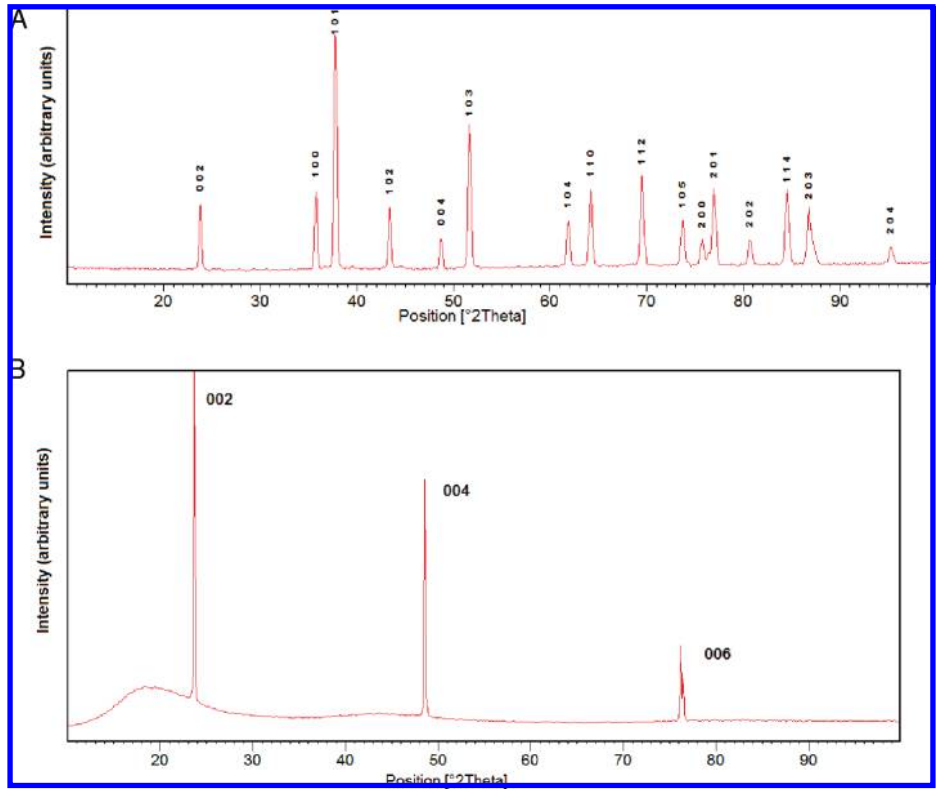


***Figure 2.*** (A) Powder diffraction pattern of crushed $ReB_2$ crystals. The pattern is indexed according to JCPDS 00-011-0581. (B) Powder X-ray diffraction pattern of an as-grown $ReB_2$ crystal oriented with respect to the *c*-axis. The large amorphous envelope at $2\theta = 20°$ is attributed to the epoxy resin encasing the crystal.

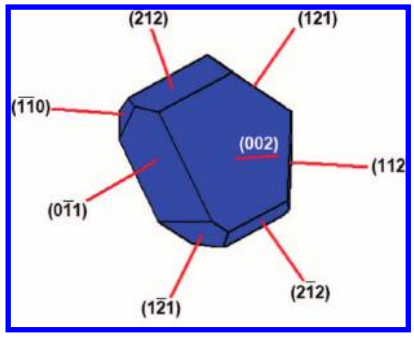


***Figure 3.*** Schematic of the terminating crystallographic planes on a flux-grown $ReB_2$ crystal determined using single crystal diffraction.

Further elemental analysis indicated that no oxygen was present in the crystals (0.000%). However, aluminum inclusions comprised 1.1 atom % of the metal concentration, resulting in an actual composition of $ReAl_{0.011}B_{1.85}$, although what sites the aluminum atoms occupy in the lattice is not known. This is to be expected when synthesizing crystals via the flux method, especially when using molten metals. The inclusion of flux into the crystal lattice has been previously reported for various other boride syntheses.[21,24,25]

**Hardness.** Vickers hardness was determined by taking the average value for the diagonals of the residual indentation and solving for hardness according to eq 1:

$$H_V = \phi \frac{P}{d^2} \quad (1)$$

where $d$ is the indentation length of the diagonal (mm), $P$ is the applied load (kg), and $H_V$ is the Vickers hardness (kg/mm$^2$). The constant $\phi$ is a geometric factor dependent on the specific indenter geometry in order to allow conversion of the measured diagonal into contact area, and it has a value of 1.8544 for a Vickers indenter. More recently, hardness values have begun to be reported in gigapascals (GPa). To convert from kg/mm$^2$ to GPa, the values obtained from eq 1 must be multiplied by a factor of 0.009807. Microindentation results for the $ReB_2$ crystals are shown in Figure 4. Indentations were made on the (002) plane and the plane perpendicular to the *c*-axis in order to determine the hardness anisotropy. Indexing of the direction cut perpendicular to the basal plane by single crystal diffraction was inconclusive; however, because the angle between these two planes was measured to be 90°, this plane will be referred to as (*hk*0). Both lattice planes exhibit the phenomenon of load-dependent hardness, known as the indentation size effect (ISE). This effect was previously observed in polycrystalline ingots of $ReB_2$ and is commonly attributed to strain gradient plasticity under the indenter.[9] Under low load, the (002) plane exhibits a maximum hardness value of 40.5 ± 2.4 GPa, approximately 6% higher than the hardness of the (*hk*0) plane. This value steadily decreases, reaching a minimum hardness under the maximum applied load, 4.9 N, at which point the values for both lattice planes converge to a hardness of ~28 GPa. The reason the two different planes exhibit anisotropic behavior exclusively under low load is likely due to the masking of the primary slip system at high load.[26] At higher indentation test forces, plastic flow occurs on multiple slip systems in order to compensate for the increase in deformed volume under the

(24) Higashi, I.; Takahashi, Y.; Atoda, T. *J. Cryst. Growth* **1976**, *33*, 207–211.

(25) Nakano, K.; Hayashi, H.; Imura, T. *J. Cryst. Growth* **1974**, *24*, 679–682.

(26) Aguilar-Santillan, J. *Acta Mater.* **2008**, *56*, 2476–2487.

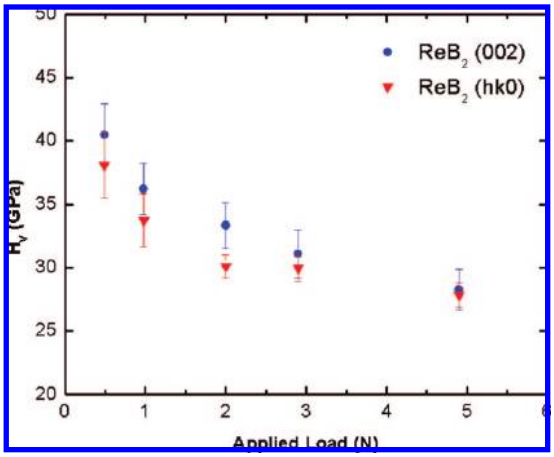


***Figure 4.*** Vickers hardness for the (002) plane (blue circles) and the (*hk*0) plane (red triangles) of $ReB_2$ flux-grown crystals. The hardness increases with decreasing load, reaching a maximum of 40.5 GPa for the (002) plane under a load of 0.49 N.

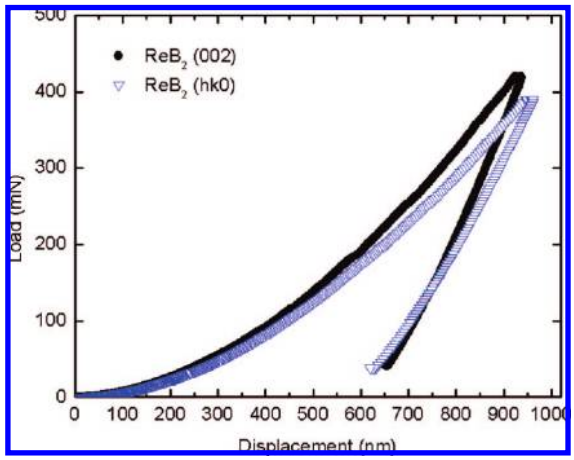


***Figure 5.*** Load vs displacement data collected using a Berkovich diamond nanoindenter for the (002) plane (solid circles) and the (*hk*0) plane (open triangles) of flux-grown $ReB_2$ crystals. For a given load, the diamond tip penetrates deeper into the (*hk*0) plane, indicative of a lower hardness for that direction.

indenter. The presence of multiple slip mechanisms masks the hardness anisotropy characteristic of only one active slip system, which differs for each lattice plane under low load.

Nanoindentation data are reported in Figure 5 for $ReB_2$ crystals. The reported values were obtained from penetration of the Berkovich diamond nanoindenter 200−800 nm beneath the specimen surface. Once again, indentation experiments were performed on the two sets of perpendicular planes: (002) and (*hk*0). The hardness measured along (002) is 36.4 ± 0.2 GPa, while the hardness of the (*hk*0) plane is 7% smaller with a value of 34.0 ± 1.3 GPa. The difference in hardness between perpendicular planes for the nanoindentation data is in good agreement with the Vickers microindentation anisotropy reported above.

Note that the low load micro- and nanohardness data reported here are lower than the values reported for arc-melted $ReB_2$[9,27] by 15% and 2%, respectively. Similarly, Lyashchenko et al. reported a Vickers hardness of 37.2 GPa under a load of 0.98 N for zone-melted $ReB_2$ compared to the 36.2 GPa obtained here for the (002) plane of flux-grown $ReB_2$ under an equivalent load.[18] Part of the decrease in hardness can be attributed to the boron-deficient structure of the flux-grown crystals. Additionally, the smaller lattice parameters presented above suggest a higher vacancy of boron atoms compared to arc-melted $ReB_2$ ($a = 2.900$, $c = 7.478$).[9] A 7.25% reduction in the number of boron atoms in the crystal (1.85/2.00) would reduce the extent of covalent bonding between the rhenium and boron atoms (the reason for the higher hardness of $ReB_2$ relative to other materials)[15] and lower the measured hardness values. Furthermore, single crystals tend to have lower hardness than polycrystalline samples because of the lack of grain boundaries, which serve to inhibit crack propagation and therefore increase hardness.[28,29]

In our previous work, we predicted that the (002) plane should be the hardest crystallographic direction in $ReB_2$ because of the layered nature of the compound and the covalent bonding of Re and B atoms between layers.[9] This hypothesis was supported by evidence from preliminary hardness data and electron backscattering diffraction, indicating a trend toward increased hardness along the direction oriented perpendicular to the *c*-axis. Additionally, incompressibility data and lattice-dependent high-pressure radial diffraction experiments indicated that the *c*-axis compresses the least under hydrostatic stress and supports the greatest degree of shear stress, respectively.[9] The results presented here confirm that the (002) plane is, in fact, the hardest direction.

Hardness anisotropy as a function of crystallographic direction has been reported in the literature for various other diborides. Studies on crystals of IVa, Va, and VIa transition metal diborides synthesized by both flux and FZ methods reveal that anisotropy in hardness measurements is related to crystal morphology and orientation during growth.[30−32] The largest crystal planes at a given temperature exhibited the highest hardness. For example, FZ crystals of $TiB_2$ and $VB_2$, both of which have hexagonal $AlB_2$-type structures, were observed to be harder in the *c*-plane (00*l*) direction compared to the *a*-plane (100) direction and grew along the *c*-axis. Similar results were found for $ZrB_2$ and $HfB_2$ crystals. The data for $ReB_2$ flux crystals coincide with these observations and confirm that the (002) plane is the hardest plane in $ReB_2$.

**Indentation Modulus.** The higher hardness of (002) compared to (*hk*0) is expected to be related to the anisotropy of the Young's moduli of specific crystallographic directions. To confirm this theory, the nanoindentation data have also been used to calculate elastic moduli. Due to the lack of an experimentally determined Poisson's ratio, the theoretically calculated[15] value of $\upsilon = 0.18$ was used for $ReB_2$ in addition to the standard values of $\upsilon = 0.07$ and $E = 1140$ GPa for diamond, as described previously by Oliver and Pharr.[20] An indentation modulus of 675 ± 7 GPa for the basal plane of $ReB_2$ was calculated over the defined range of 200−800 nm; the corresponding value for the perpendicular plane is 510 ± 13 GPa. The anisotropy present in the indentation moduli is consistent with both the nano- and microindentation hardness values, with the *c*-axis possessing a higher hardness and greater indentation modulus than the (*hk*0) plane.

Determination of the elastic moduli by nanoindentation is based on the theory of contact mechanics for elastically *isotropic*

(27) Chung, H.-Y.; Weinberger, M. B.; Yang, J.-M.; Tolbert, S. H.; Kaner, R. B. *Appl. Phys. Lett.* **2008**, *92*, 261904.
(28) Hall, E. O. *Proc. Phys. Soc. London, Sect. B* **1951**, *64*, 747–753.
(29) Petch, N. J. *J. Iron Steel Res. Inst.* **1953**, *174*, 25–28.
(30) Otani, S. *J. Ceram. Soc. Jpn.* **2000**, *108*, 955–956.
(31) Otani, S.; Korsukova, M. M.; Mitsuhashi, T. *J. Cryst. Growth* **1998**, *194*, 430–433.
(32) Otani, S.; Xuan, Y.; Yajima, Y.; Mori, T. *J. Alloys Compd.* **2003**, *361*, L1–L3.

materials.[20,33] Consequently, the indentation moduli calculated here are expected to differ from the Young's modulus because of the anisotropy inherent in the layered lattice of $ReB_2$. The Young's modulus in the direction of the indentation will dominate the elastic response; however, the indentation modulus will also be partially dependent on the other elastic constants.[33] Thus, the elastic anisotropy present in $ReB_2$ crystals measured by nanoindentation can be reconciled with the elastic constants determined by first-principle calculations.[15] The calculated elastic stiffness constants, $C_{11}$ and $C_{33}$, which are also highly anisotropic, measure the resistance to linear compression along the *a* and *c*-axes, respectively. The constant for the *c*-axis, $C_{33}$, has the largest value (approximately 1100 GPa), which explains the higher indentation modulus along this direction.

The elastic moduli differ by 25% compared to only 6% for the hardness values for (002) and (*hk*0). This difference in anisotropy can also be explained by careful manipulation of the elastic constants. Hao et al.[15] calculated the ratio of the linear compressibility coefficients for the *c* and *a*-directions:

$$k_c/k_a=(C_{11}+C_{12}-2C_{13})/(C_{33}-C_{13}) \quad (2)$$

which is indicative of the degree of compressional anisotropy, with unity indicating an isotropic material.[34] Similarly, the shear anisotropy ratio can be calculated according to eq 3:[34]

$$A=2C_{44}/(C_{11}-C_{12}) \quad (3)$$

$ReB_2$ has values of $k_c/k_a = 0.56$ and $A = 1.06$. These numbers indicate that elastic compression is more anisotropic than shear. Numerous studies have shown that hardness is more highly correlated with shear strength than compressive strength.[35−38] Therefore, we expect hardness to be more isotropic than the elastic modulus, which is observed experimentally. The greater degree of anisotropy present for indentation moduli compared to hardness indicates different mechanics giving rise to elastic and plastic deformation and suggests that mechanical anisotropy is reduced in the presence of plastic deformation.

**Electrical Resistivity.** In-plane electrical resistivity ($\rho_{ab}$) measurements performed on $ReB_2$ crystals are shown in Figure 6, and electrical resistivity values for various other hard materials are listed in Table 1 for comparison. $ReB_2$ exhibits metallic conductivity, as its conductivity increases with decreasing temperature. A room temperature resistivity of $\rho_{ab}(300K) = 45 \pm 15\ \mu\Omega\cdot$cm was measured, and impurity scattering accounts for a residual resistivity of $\rho_{ab}(0) = 3.5(1)\ \mu\Omega\cdot$cm and a residual resistivity ratio of 13. These results are consistent with the recent theoretical calculations predicting that $ReB_2$ is metallic with a nonzero density of states at the Fermi level due to overlap of the 2p orbitals of B with the 5d orbitals of Re.[15] To the best of the authors' knowledge, $ReB_2$ is the hardest bulk material possessing metallic conductivity, with a Vickers hardness considerably higher than those of any of the other materials present in Table 1.

**Magnetic Susceptibility.** Magnetic susceptibility measurements confirm the absence of superconductivity down to 2.0 K, in accordance with the findings of Kawano et al.[39] $ReB_2$ crystals are paramagnetic with a Curie-tail at low temperatures.

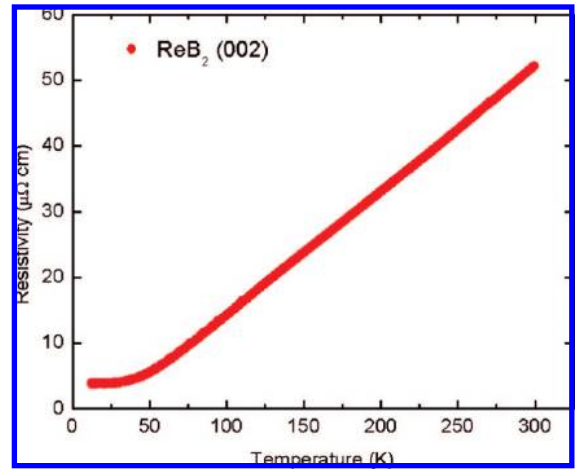


***Figure 6.*** Resistivity vs temperature for a $ReB_2$ crystal measured along the (002) plane. $ReB_2$ exhibits metallic conductivity with a room temperature resistivity of $\rho_{ab}$ (300) = 40.7 $\mu\Omega\cdot$cm and a residual resistivity ratio = 13.

***Table 1.*** Electrical Resistivity and Vickers Hardness Values for Various Hard and Superhard Compounds

| compd | resistivity at 300 K, $\rho_{ab}$ ($\mu\Omega\cdot$cm) | Vickers hardness (GPa)[a] |
|---|---|---|
| $ReB_2$ | 40.7[b] | 40.5[b] |
| $TiB_2$ | 28.4[c] | 33.3[d] |
| HfC | 109[c] | 28.1[d] |
| WC | 53[c] | 23.5[d] |
| $B_4C$ | 760000[e] | 23.5[d] |
| TiN | 21.7[c] | 20.6[f] |

[a] Hardness values are reported under a load of 50 gf; load for $B_4C$ not reported. [b] This work. [c] Schwarzkopf, P.; Kieffer, R. *Refractory Hard Metals*; Macmillan Company: New York, 1953. [d] Shackelford, J. F., Alexander, W., Eds.; CRC Materials Science and Engineering Handbook, 3rd ed.; Boca Raton, FL, 2001. [e] Meerson, G. A.; Kiparisov, S. S.; Gurevich, M. A.; Feng-Siang, D. Poroshk. Metall. **1965**, *27*, 62−68. [f] Reference 23.

**Thermal Stability.** Thermogravimetric data are presented in Figure 7 for a flux-grown $ReB_2$ crystal weighing 21.95 mg and 14.5 mg of $ReB_2$ (nominal composition) powder synthesized via an elemental solid-state reaction. Upon heating in dry air, the $ReB_2$ powder exhibits a very slight drop in mass at 100 °C, corresponding to the loss of absorbed water. At 600 °C, a large exothermic peak presents itself in the DTA curve as the powder begins to lose a significant portion of its mass. The mass loss continues until the completion of the run, totaling over 50% of the original sample mass. Due to the fact that boron comprises only 10 mass % of $ReB_2$, the change in weight can be attributed primarily to the loss of rhenium by the formation of volatile $ReO_3$ plus some loss of boron by the formation of $B_2O_3$. Initially, the $ReB_2$ crystal responds similarly to heating in air, with a small drop in mass at 100 °C. However, no further change is observed until approximately 800 °C, when the crystal loses a small percentage of mass. Note that if the flux crystal is heated at a slower rate (2 °C/min) up to 1000 °C, the mass loss increases accordingly, totaling 1.5% of the original sample weight.

Visual inspection of the crystal after heating indicates the presence of a glassy coating. Sonication in methanol removed

(33) Hay, J. C.; Sun, E. Y.; Pharr, G. M.; Becher, P. F.; Alexander, K. B. *J. Am. Ceram. Soc.* **1998**, *81*, 2661–2669.
(34) Steinle-Neumann, G.; Stixrude, L.; Cohen, R. E. *Phys. Rev. B* **1999**, *60*, 791.
(35) Teter, D. M. *MRS Bull.* **1998**, *23*, 22.
(36) Brazhkin, V. V.; Lyapin, A. G.; Hemley, R. J. *Philos. Mag. A* **2001**, *82*, 231.
(37) Leger, J. M.; Djemia, P.; Ganot, F.; Haines, J.; Pereira, A. S.; da Jornada, J. A. H. *Appl. Phys. Lett.* **2001**, *79*, 2169.
(38) Gilman, J. J.; Cumberland, R. W.; Kaner, R. B. *Int. J. Refract. Met. Hard Mater.* **2006**, *24*, 1–5.
(39) Kawano, A.; Mizuta, Y.; Takagiwa, H.; Muranaka, T.; Akimitsu, J. *J. Phys. Soc. Jpn.* **2003**, *72*, 1724–1728.

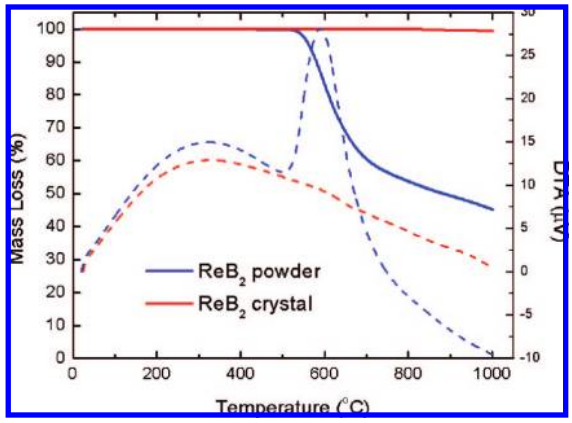


***Figure 7.*** Thermogravimetric data for $ReB_2$ powder (blue lines) and a $ReB_2$ crystal (red lines). The crystal loses a negligible amount of mass (solid line) compared to the case of the powder, which undergoes rapid decomposition at 600 °C, as indicated by the weight loss and large exothermic peak in the DTA curve (dashed lines).

the layer and restored the crystal to its previously lustrous appearance. The enhanced stability of the $ReB_2$ crystal is likely due to the leaching out of boron from the lattice. The boron then reacts with atmospheric oxygen to form a protective surface coating of $B_2O_3$ ($B_2O_3$ is soluble in methanol) that drastically lowers the rate at which any further oxidation might occur. The thermal response of $ReB_2$ is contrasted with the behavior of other borides that tend to form stable transition metal oxides upon heating, resulting in weight gains ranging from a few percent ($WB_2$) to an excess of 20% ($TaB_2$).[21,40]

## Conclusions

We have reported the synthesis of superhard $ReB_2$ crystals by a flux method using molten aluminum. The crystals grow oriented along the *c*-axis and exhibit directional anisotropy. Indentation measurements of the (002) and (*hk*0) planes of $ReB_2$ show that the (002) plane is the hardest crystallographic plane, with the highest indentation modulus. Thermogravimetric analysis indicated enhanced thermal stability of $ReB_2$ crystals up to 1000 °C. Resistivity measurements demonstrated that $ReB_2$ is a conducting material.

$ReB_2$ is the only bulk superhard material so far to exhibit metallic behavior. Most superhard materials are insulators because of the large band gap that results from strong covalent bonding and filling of the bonding orbitals, while leaving the antibonding orbitals unoccupied. The band gaps for diamond and cubic boron nitride are $E_g = 5.4$ eV and $E_g = 6.4$ eV, respectively, compared to 0 eV for $ReB_2$.[41,42] The resistance of $ReB_2$ crystals to thermal degradation and their ability to freely conduct electricity paves the way for development of superhard coatings with technical capabilities for use in the defense and aerospace industries.

**Acknowledgment.** The authors would like to thank Dr. E. Sung for use of the microindenter, Dr. Saeed Khan for crystal structure determination, Dr. Amir Liba for chemical analysis, and Dr. Danielle Gray (Northwestern University) for help with the Rietveld refinement. This work was funded by the National Science Foundation under Grants DMR-0453121 (R.B.K.), DMR-0805357 (R.B.K.), and DMR-0520552 (S.E.B.) and an Integrative Graduate Education and Research Traineeship (J.B.L., J.A.W.).

JA804989Q

(40) Okada, S.; Kudou, K.; Higashi, I.; Lundstroem, T. *J. Cryst. Growth* **1993**, *128*, 1120–4.
(41) *CRC Handbook of Chemistry and Physics*, 88th ed.; CRC: 2007−2008.
(42) Chrenko, R. M. *Solid State Commun.* **1974**, *14*, 511–515.